# Edge turbulence and flows in the presence of Resonant Magnetic Perturbations on MAST

**P Tamain[1]‡ , A Kirk[1], E Nardon[1], B Dudson[2], B Hnat[3] and the MAST team[1]**

[1] EURATOM/CCFE Fusion Association, Culham Science Centre, Abingdon, Oxon, OX14 3DB, UK

[2] Physics Department, University of York, YO10 5DD, UK

[3] Centre for Fusion, Space and Astrophysics, Department of Physics, Warwick University, Coventry CV4 7AL, UK

E-mail: patrick.tamain@ccfe.ac.uk

**Abstract.** The impact of Resonant Magnetic Perturbations (RMPs) on the edge of MAST L-mode plasmas is studied using a mid-plane reciprocating probe equipped with a Gundestrup probe head. A strong impact on the characteristics of the ion saturation current fluctuations is observed just inside the separatrix, with a broadening of the power spectrum and an asymmetrization of the probability distribution functions towards non-gaussian shapes. No major effect is found in the Scrape-Off Layer (SOL). Floating potential measurements are used to evaluate the modification of the plasma potential profiles. The radial electric field profile flattens when RMPs are applied, leading to a theoretically expected increase inside the separatrix and a decrease in the SOL. A consistent change is observed on the perpendicular and parallel flows which tend to increase inside the separatrix. On the contrary, in the SOL, a braking of the rotation is observed with the application of RMPs. All these effects occur only above a threshold in the amplitude of the current applied in the RMP coils and and are not toroidally localized.

PACS numbers: 52.55.Fa, 52.30.-q, 52.35.Ra, 52.70.Ds

‡ Present address: Association Euratom-CEA, Institut de Recherche sur la Fusion Magnétique, CEA Cadarache, F-13108 St. Paul-lez-Durance, France

## 1. Introduction

The mitigation of large type I Edge Localized Modes (ELMs) remains an unavoidable milestone on the way to ITER [1]. Among the various methods foreseen as possible candidates to achieve that goal, the use of Resonant Magnetic Perturbations (RMPs) coils on the DIII-D tokamak is the only one which has demonstrated full ELM suppression [2, 3, 4, 5]. Encouraging results have also been obtained on JET where an increase of the ELM frequency and associated drop of their amplitude has been observed when applying perturbations with the external error field correction coils [6, 7].

The idea underlying those experiments is to generate a stochastic magnetic field layer in the pedestal region in order to increase locally the radial transport and keep the pedestal pressure gradient below the threshold of the peeling-ballooning modes that are thought to be the dominant mechanism in the development of ELMs [8, 9]. In DIII-D, experiments have shown a correlation between ELM suppression and the degree of overlapping of the generated magnetic islands predicted by vacuum field modelling (computation of the magnetic equilibrium without taking into account the plasma response to the perturbation). However, in the absence of a fully consistent and predictive model, the viability of the method needs to be assessed experimentally on other machines in order to allow extrapolation to ITER.

The MAST spherical tokamak has recently been equipped with a set of RMP coils (or ELM Control Coil, ECC) [10]. At the present time, no ELM suppression has been observed even though vacuum modelling predicts a stochastization of the magnetic field lines larger than the threshold found on DIII-D [11]. Moreover, recent theoretical results [12, 13, 14] indicate that the response of the plasma to the magnetic perturbation could strongly screen the RMPs so that the stochastization expected from the vacuum modelling may actually not occur in the plasma.

In that perspective, experiments in L-mode plasmas constitute a useful input to shed more light on the subject and help to isolate the fundamental mechanisms at play in the plasma response, with the advantage of being easier to diagnose. Moreover, a large amount of data has been gathered in the last 20 years on the effect of stochastic boundary layers on tokamaks equipped with so-called ergodic divertors [15, 16, 17, 18], thus allowing a comparison of results with those published in the literature.

In this article, we present results obtained with the MAST fast reciprocating probe, focusing on the impact of the RMPs on the edge turbulence, flows and radial electric field in L-mode plasmas. Similar studies on TEXT [15], Tore Supra [19, 20] and TEXTOR [21, 22, 23] have demonstrated a strong impact of a stochastic field layer on the fluctuation level and their characteristics (Probability Distribution Function (PDFs), spectra...). Of particular interest is the evolution of the radial electric field which is expected theoretically to increase in the presence of RMPs in order to preserve the ambipolarity of the plasma [22, 24, 25].

This paper is organized as follows: the experimental setup is described in section 2, results are presented in section 3, discussed in section 4 and conclusions drawn in

section 5.

## 2. Experimental setup

### *2.1. The MAST ELM Control Coils*

The ECC system installed on MAST consists of two rows of six in-vessel coils producing $n = 3$ perturbations . They were dimensioned to satisfy the ELM suppression threshold suggested by the experiments on DIII-D [10]. Each of the coils is made of 4 turns and can be driven with a maximum current of $5.6kAt = 1.4kA \times 4$ turns. The $n = 3$ symmetry is obtained by powering neighbouring coils in the toroidal direction with opposite currents (+-+-+- for example). The wiring of the coils allows for some flexibility in the shape of the perturbation: according to the relative signs of the currents flowing through the top and bottom coils, the ECCs will be said to run in even (same current signs in the upper and lower coils at a particular toroidal location) or in odd (opposite currents) configuration. Reversing the current in all the coils in one row (ie -+-+-+ instead of +-+-+-) leads to a toroidal phase shift of 60°, so that each of the two previous configurations can be run in 0° or 60° phase.

### *2.2. Gundestrup reciprocating probe head*

The measurements presented in this paper were obtained with the MAST mid-plane reciprocating probe [27] equipped with a Gundestrup probe [28]. Fig. 1 shows a photograph as well as a schematic drawing of the probe head used. It consists of two groups of graphite pins distributed at the end of a 5cm diameter boron nitride cylinder coated with coloidal graphite. Pins 1 to 8 are uniformly distributed around the cylinder. They are flush to the surface 3.5mm behind the front plane of the probe and have a diameter of 2.85mm. In the set of experiments described here, they were biased to -200V to measure the ion saturation current $I_{sat}$. The three remaining pins (9 to 11) are located at the front of the probe head and stick out of its front plane by 1.5mm. Their diameter is 1.35mm for pins 9-10 and 4.85mm for pin 11. They were used to measure the floating potential $V_{fl}$.

### *2.3. Scenarios*

The reference scenario for all the results presented here is a $I_p = 400kA$ ohmic L-mode discharge in connected double null (CDN) configuration. Fig. 2 shows the time evolution of the main plasma parameters for shots #21712 to #21714. Shot #21712 is the reference shot with no current applied in the ECCs, $I_{coils} = 0$. In shots #21713 and #21714, the ECCs are turned on at 0.3s, reaching their flat-top current (respectively $I_{coils} = 1.4kA$ and $I_{coils} = 1kA$) at 0.32s before being ramped down between 0.455s and 0.48s (Fig. 2 (c)). The coils are configured in even 60° phase configuration. As already reported in [11, 29], a clear effect of the RMPs is found on the plasma density with a

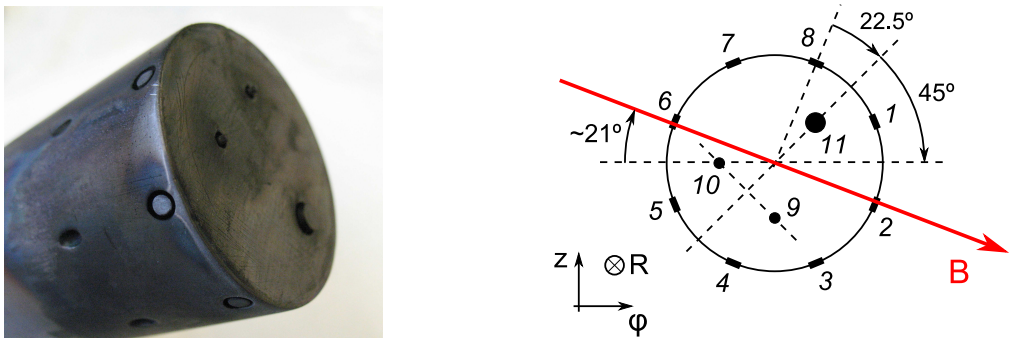


**Figure 1.** The Gundestrup probe head used on the MAST fast reciprocating probe. (a) Photograph of the Gundestrup probe head ; (b) schematics of the probe head as seen from inside the vessel in the radial direction. The typical direction of the magnetic field in the experiments described here is also indicated.

drop of the line-averaged density of the plasma (Fig. 2 (b)) reminiscent of the density pump-out observed in DIII-D [3] and JET [6, 7] in H-mode. The density pump-out is associated with an increase of the $D_\alpha$ signal in the lower divertor also visible in Fig. 2 (b), suggesting an increase of the particle transport to the divertor. Consistent with the density data, the change in the $D_\alpha$ signal in #21714 is much less noticeable than in #21713.

The reciprocating probe was plunged in each of these discharges up to 3.5cm inside the separatrix, reaching its deepest position at the time when the ECCs were turned on (Fig. 2 (d)). It then reciprocated back during the duration of the ECCs current flat-top, thus measuring radial profiles on its way out. In the rest of the paper, the radial position of the probe $r_{probe}$ (or $r$ when no confusion is possible) refers to the front plane of the probe head. It is most often referred to with respect to the position of the separatrix $r_{sep}$ which is determined from the peak radius of the $D_\alpha$ emission of the plasma ($r_{sep} = r_{D_\alpha peak} + 1cm$, which is also used as a constraint for the magnetic reconstruction). Altogether, the localization of the probe with respect to the last closed flux surface is known with a precision of the order of 1cm. The pitch angle of the magnetic field lines at the position of the reciprocating probe (reconstructed by EFIT [30]) depends on its radial position, ranging from 18° at the outermost position to 22° at the deepest point. The alignment of the Gundestrup probe pins with the magnetic field is illustrated on Fig. 1 for a pitch angle of 21° corresponding to the situation 1cm inside the separatrix.

Note that most of the data presented in this paper are taken out of the triplet of shots #21712 to #21714. The reported phenomena have however been observed in many other discharges based on the same scenario. In the following section, we focus mainly on the 3 shots shown on Fig. 2 because they happen to be the ones that had the best simultaneous diagnostic coverage.

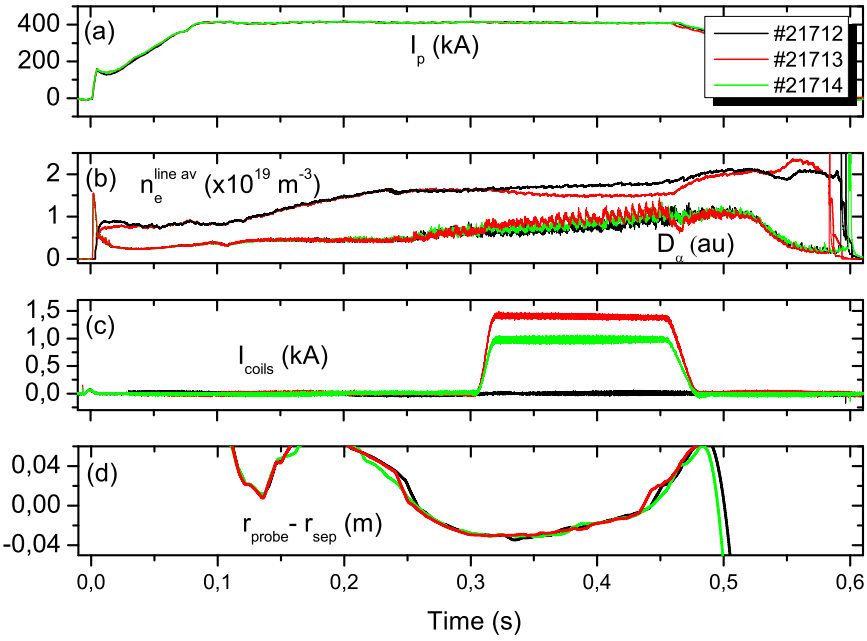


**Figure 2.** Time evolution of plasma parameters in shots #21712 to #21714. (a) Plasma current; (b) line averaged density and $D_\alpha$ emission in the lower divertor; (c) absolute value of the current driven in the ELM control coils; (d) radial position of the fast reciprocating probe head in the outer mid-plane $r_{probe}$ with respect to the position of the separatrix $r_{sep}$.

## 3. Experimental result

### *3.1. Evolution of the ion saturation current level and fluctuations*

Fig. 3 shows extracts of the $I_{sat}$ signals measured by 4 of the pins (1 to 4) around $t = 0.35s$ (a) and $t = 0.45s$ (b) for the 3 considered shots. At those times, the probe is located respectively at $r - r_{sep} \simeq -3cm$ and $r - r_{sep} \simeq +2cm$ and the ECCs are energized in #21713 ($I_{coils} = 1.4kA$) and #21714 ($I_{coils} = 1kA$). Several observations can be made from these data. First of all, the ECCs at their maximum current (1.4kA) induce a change of the average level of the $I_{sat}$ signal for some, but not all, of the pins of the Gundestrup probe. This is illustrated in Fig. 3 (c) that shows the relative variation of the fluctuation-averaged ion saturation current signals (averaged over a 5ms sliding window) between shot #21712 and shot #21713. Before the onset of the RMPs (ie on the way in of the probe), no noticeable difference is visible between the two shots. On the contrary, once the coils are energized, one can observe a clear drop of the $\langle I_{sat} \rangle$ signal inside the separatrix, but with a different amplitude for each of the pins of the Gundestrup probe. For example, in the case of pin 2 3cm inside the separatrix, the relative amplitude of the decrease is found to be comparable to the amplitude of the

density pump-out (of the order of 15%). On the other hand, pin 8 at the same radial location does not exhibit a major change of $\langle I_{sat} \rangle$ while pin 4 does show a drop of 60% at the same radial location. Thus, the modification of the amplitude of the ion saturation current cannot be purely explained by the density pump-out. Such an asymmetry in the evolution of the signals of the various pins of the Gundestrup probe also suggests a change in the edge plasma flows. We will come back to that point later. In the SOL ($r - r_{sep} > 0$), no obvious change of the fluctuating signals is visible in Fig. 3 (b). When looking closer however, the average level of $I_{sat}$ is found to increase by a factor ranging from 10% to 40%, with again different values for the different pins (see Fig. 3 (c)). The transition between the zone where $\langle I_{sat} \rangle$ drops and the one where $< I_{sat} >$ increases with the RMPs occurs in the vicinity of the separatrix across a layer of the order of 1cm thick.

A clear effect of the RMPs on the fluctuations themselves is also visible in Fig. 3 (a) and (b). On $I^1_{sat}$ and $I^2_{sat}$ for example, the onset of the ECCs at 1.4kA is correlated with the appearance of "holes" in the signals when the probe is located inside the separatrix, as well as a drop of the time scale of the fluctuations. This suggests a modification of both the power spectrum and the PDF.

The normalized power spectra of the 8 $I_{sat}$ signals are given in Fig. 4 for two radial positions of the Gundestrup probe, 3cm inside the separatrix (top) and 2cm outside in the SOL (bottom). At the maximum current, a strong broadening of the spectra is

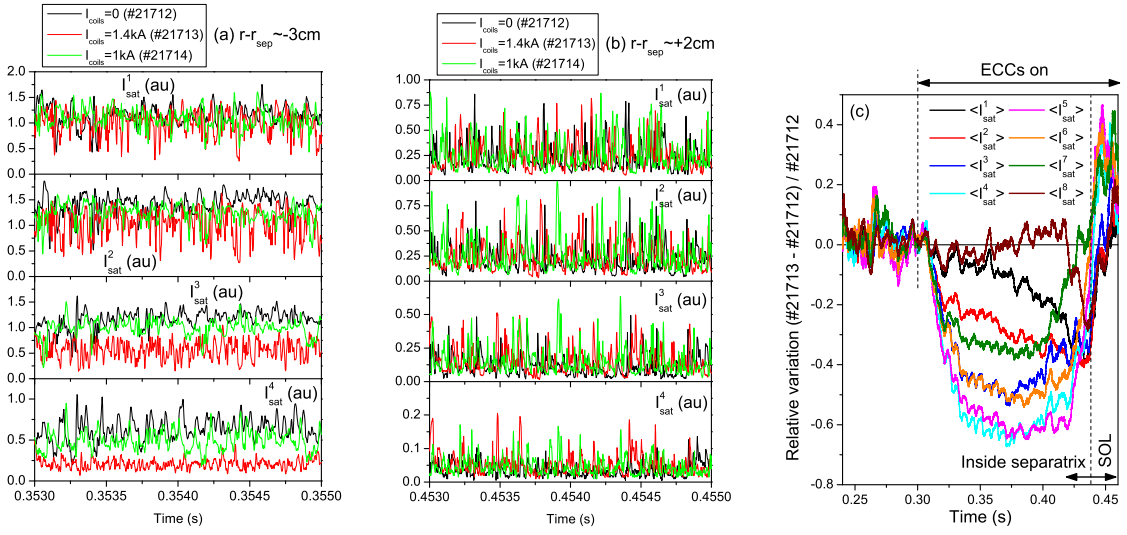


**Figure 3.** Extracts of the time evolution of the ion saturation current signal for pins 1 to 4 of the Gundestrup probe head in shots #21712 to #21714: (a) when the probe is located 3cm inside the separatrix; (b) when the probe is located in the Scrape-Off Layer 2cm outside the separatrix. (c) Time evolution of the relative variation of the averaged ion saturation current signals (over a 5ms sliding window) for pins 1 to 8 during the plunge of the probe in shot #21713 (ECCs energized at 1.4kA) with respect to shot #21712 (no current in the ECCs).

visible on all the pins in the closed field lines region, suggesting an enhancement of small scale turbulence. By integrating over the spectrum, we can get the RMS fluctuations level:

$$\frac{\delta I_{sat}}{\langle I_{sat}\rangle} \equiv \sqrt{\frac{\langle \delta\left(I_{sat}-\langle I_{sat}\rangle\right)^2\rangle}{\langle I_{sat}\rangle^2}} = \sqrt{\int_{f\neq 0}\left|\frac{\widehat{I}_{sat}\left(f\right)}{\widehat{I}_{sat}\left(0\right)}\right|^2 df} \tag{1}$$

This level is typically almost doubled inside the separatrix when the maximum perturbation is applied, increasing from 13-21% without the RMPs to 21-32% with the ECCs driven at 1.4kA, depending on the considered pin. This is illustrated in Fig. 5, which shows the radial profiles of the fluctuation level of the ion saturation current signal on pin 2 $I_{sat}^2$ for the 3 considered shots. At 1kA however, these effects, although visible, remain very limited. This observation demonstrates either the existence of a threshold in the amplitude of the RMPs to get an effect on the turbulence in the edge plasma or at least a strong non linearity of the effect as a function of $I_{coils}$. Such a behaviour has already been established for the density pump-out [11]. A similar broadening of the density fluctuation spectrum was observed in the pedestal of DIII-D H-mode discharges during ELM control experiments [31]. Although an increase of the fluctuation level does not necessarily imply an increase of the turbulent transport, these results can be correlated with recent transport simulations that showed that a local increase of the turbulent transport level just inside the unperturbed separatrix is necessary to recover the density pump-out [32].

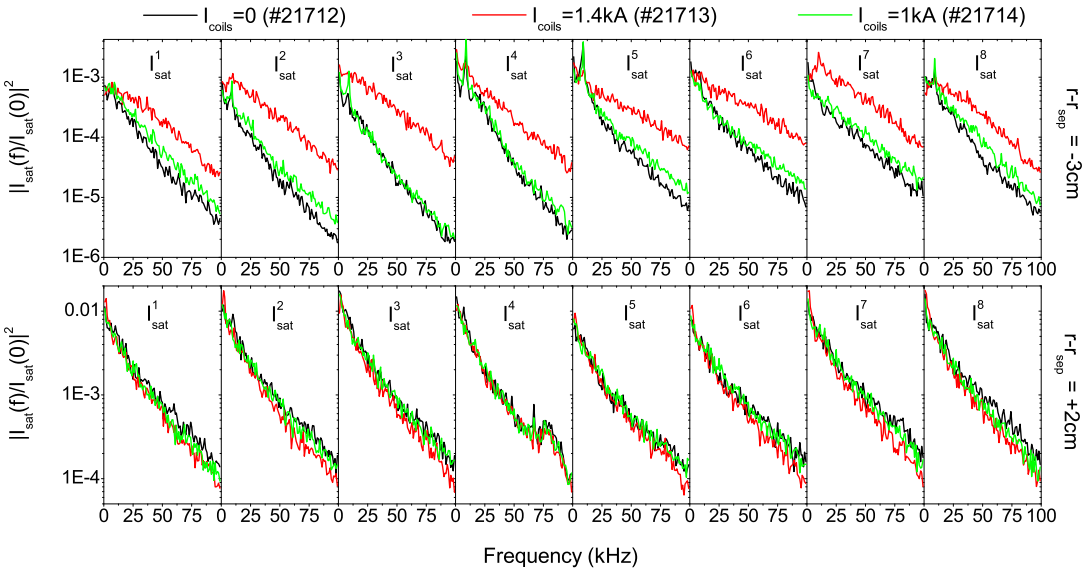


**Figure 4.** Normalized power spectra of the ion saturation current signals ($\left|\frac{\widehat{I}_{sat}(f)}{\widehat{I}_{sat}(0)}\right|^2$) for the 8 $I_{sat}$ pins of the Gundestrup probe head at two radial positions: top row, 3cm inside the separatrix; bottom row, 2cm outside the separatrix in the SOL.

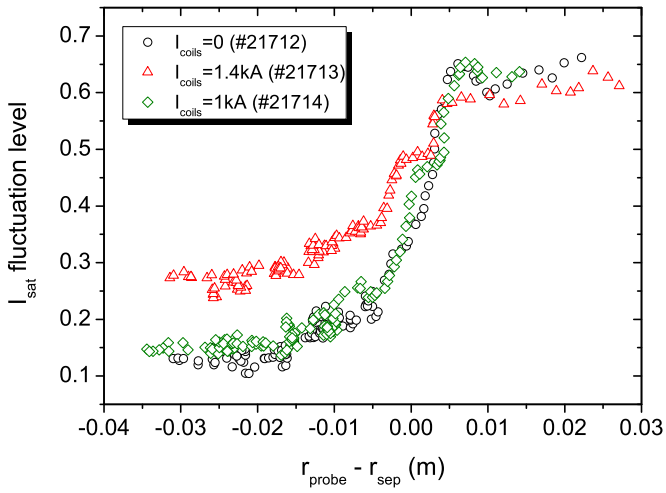


**Figure 5.** Radial profile of the fluctuation level of the ion saturation current signal on pin 2 as measured by the Gundestrup probe on its way out in shots #21712 ($I_{coils} = 0$), #21713 ($I_{coils} = 1.4kA$) and #21714 ($I_{coils} = 1kA$).

Further out in the plasma, the effect of the RMPs on the spectra tends to vanish and eventually slightly reverses in the SOL. This is visible in Fig. 4 (bottom) in which a slight decrease of the bandwidth can systematically be noticed when the ECCs are used at full current. As a consequence, the fluctuation level decreases in this region, from 50-75% without the RMPs to 45-65% with the ECCs at 1.4kA. Once again, almost no effect is observed at $I_{coils} = 1kA$.

Let us now look at the impact of the RMPs on the PDFs of the $I_{sat}$ fluctuations. Fig. 6 shows the PDFs of the signals measured by the 8 pins 3cm inside the separatrix (top row) and 2cm outside the separatrix in the SOL (bottom row). In order to eliminate any distortion due to the variation of the average level of the signal and to focus on the characteristics of the fluctuations themselves, the horizontal axes have been normalized to $\langle I_{sat} \rangle$ and centered on the average value. When no current is applied in the ECCs, rather symmetric Gaussian-like distributions are found on all the pins 3cm inside the separatrix, while the PDFs 2cm out in the SOL exhibit an asymmetric shape with a dominant positive tail indicating a strongly intermittent behaviour. Such results are usual for fluctuation measurements in the edge plasma in L-mode [33]. When the ECCs are driven at 1.4kA, the PDFs of all the $I_{sat}$ signals 3cm inside the separatrix get broader and develop dominant tails. Interestingly however, all the pins do not measure the same alteration of the PDFs: for half of them (pins 8, 1, 2 and 3), it is a negative tail that develops (negative skewness), while for the other half (pins 4 to 7), it is on the positive side that the PDFs grow (positive skewness). Thus, the RMPs are responsible for the appearance of intermittency in the fluctuations inside the separatrix, but according to the pins, that intermittency can be linked either to blobs or holes travelling in the

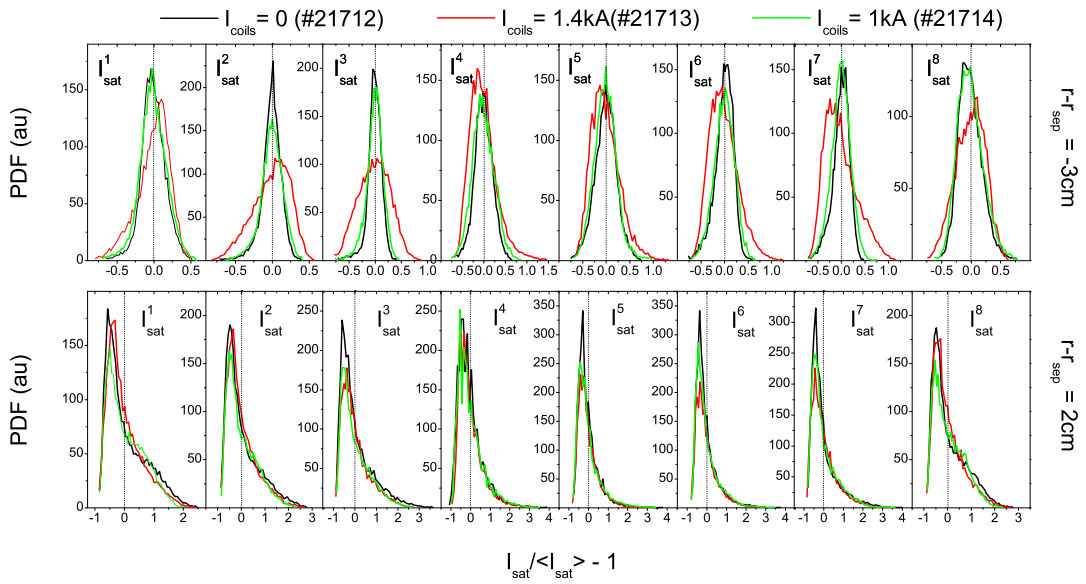


**Figure 6.** Probability Distribution Functions of the ion saturation current signals for the 8 $I_{sat}$ pins of the Gundestrup probe head at two radial positions: top, 3cm inside the separatrix; bottom, 2cm outside the separatrix in the Scrape-Off Layer.

plasma. In the SOL, little change can be noticed in the shape of the PDFs even at full current in the ECCs. Some of the pins do measure a reduction of the amplitude of the peak of the PDF, but this is not systematic and hence difficult to interpret.

### *3.2. Radial electric field*

One of the main theoretical predictions and experimental observations concerning the impact of RMPs on the edge plasma concerns its influence on the radial electric field $E_r$ [22, 24, 25]. Indeed, the existence of a stochastic layer in the edge changes the magnetic topology and field lines that would lie on a closed flux surface in the unperturbed equilibrium can be brought in contact with the divertor. Because of the difference in the thermal velocities of ions and electrons, the electron flux to the wall along those newly open field lines tends to be much larger than the ion flux. In response to that electron outflux, an additional positive radial electric field builds up in order to preserve the ambipolarity of the fluxes. This way the observation of a positive perturbation of the radial electric field, as was already reported on TEXTOR [22], can be considered as a sign of stochastization of the edge plasma.

The floating potential $V_{fl}$ measurements obtained by the front pins of the probe (9 to 11) allow an insight into the evolution of the plasma potential profiles $V_p$ during RMPs, and thus into the radial electric field. $V_p$ and $V_{fl}$ differ by the amplitude of the

sheath potential drop $\Lambda$:

$$V_p = V_{fl} + \Lambda \tag{2}$$

where $\Lambda$ is given by the classical relation $\Lambda = -\frac{1}{2}\frac{T_e}{e}\ln\left[2\pi\frac{m_e}{m_i}\left(1+\frac{T_i}{T_e}\right)\right]$ [26]. The logarithm term does not vary much with $\frac{T_i}{T_e}$ so that it is usual to approximate relation (2) by:

$$V_p \simeq V_{fl} + 2.5\frac{T_e}{e} \tag{3}$$

This formula is of course an approximation, all the more as it is now well established that the ratio $T_i/T_e$ can vary from 1 to 10 in the SOL [34]. However, we are more interested here in the evolution of the plasma potential profiles (ie the radial electric field) when RMPs are applied rather than in an absolute measurement of those quantities:

$$\Delta E_r = -\partial_r\left(\Delta V_{fl}\right) - 2.5\frac{\partial_r\left(\Delta T_e\right)}{e} \tag{4}$$

Since no measurement of $T_e$ is available from the probe data in the considered shots, Thomson Scattering data were used for electron temperature profiles. These profiles were found to be invariant within the statistical fluctuations ($\pm 5eV$) whether the ECCs are powered or not. Hence, the $\partial_r\left(\Delta T_e\right)$ term in equation (4) does not have any influence on the variation of the radial electric field and the choice of the sheath multiplicative coefficient only impacts the error bars of the measurement.

Fig. 7 (a) shows the radial profiles of the measured fluctuation-averaged (over a 5ms sliding window) floating potential for the three studied values of the current in the ECCs. The corresponding radial electric field profiles are given in Fig. 7 (b). As for the ion saturation current measurements, the $I_{coils} = 0$ and $I_{coils} = 1kA$ cases are extremely similar giving more evidence of the existence of a threshold around or slightly above $I_{coils} = 1kA$. At $I_{coils} = 1.4kA$ however, a marked increase of the plasma floating potential is observed inside the $r - r_{sep} = -1.5cm$ flux surface, with an increase from $V_f = -85V$ to $V_f = -50V$ at $r - r_{sep} = -1.5cm$. A small drop of 15V is also visible in the SOL just outside the separatrix but its significance for the plasma potential can be argued, given the order of magnitude of the error bars discussed above. Translated in terms of radial electric field, these modifications of the potential profile lead to an increase of $E_r$ in a 2cm wide layer just inside the separatrix, with a change of up to 2kV/m at $r - r_{sep} = -1cm$. This observation is in qualitative agreement with the changes in $E_r$ measured by Doppler spectroscopy [35] in the same discharges [36]. In the SOL, the possible alteration of the potential profile gives a slight shift of $E_r$ towards less positive values, but, as stated above, the reality of that effect is arguable.

### *3.3. Rotation velocities*

Gundestrup probe heads were originally designed to allow the measurement of flow velocities in the parallel as well as in the perpendicular direction [28, 40]. The relative amplitude of the $I_{sat}$ signal on the pins distributed around the head can be related to

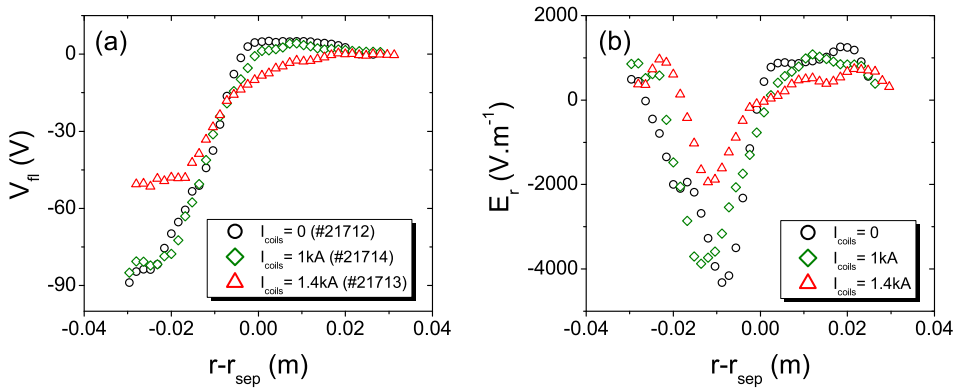


**Figure 7.** (a) Radial profiles of the fluctuation-average value of the floating potential as measured by the Gundestrup probe during the return of its reciprocation. (b) Corresponding profiles of the radial electric field as obtained from relation 4.

the parallel ($M_\parallel$) and perpendicular Mach number ($M_\perp$ - perpendicular to the magnetic field direction in the plane of the $I_{sat}$ pins), defined as the flow velocities normalized to the local acoustic velocity of the plasma $c_s = \sqrt{(T_e + T_i)/m_i}$. Several models have been proposed to interpret the data of Gundestrup probes, based either on a fluid [37, 38] or a kinetic [39] description. Those different approaches give similar predictions [40]. One must however note that these models have been established for laminar flows and that, to the authors' knowledge, no result has yet been published on the interpretation of such measurements in a strongly turbulent plasma.

In the following, we apply the Van Goubergen model [37, 41] to the fluctuation-averaged $I_{sat}$ signals. According to this approach, the ratio of the signal measured by two opposite pins is given by:

$$\frac{1}{c} \ln \left( \frac{\langle I_{sat}^{i+4} \rangle}{\langle I_{sat}^{i} \rangle} \right) = M_\parallel - \frac{M_\perp}{\tan \alpha_i} \qquad \forall i = 1..4 \tag{5}$$

where $\alpha_i$ is the incidence angle of the magnetic field line on the probe pins ($\alpha_i = 0$ for a grazing incidence, $\alpha_i = 90°$ for a normal incidence). $c$ is a parameter weakly dependent on $M_\parallel$ (ranging from 2.28 to 2.33 for $M_\parallel$ between 0 and 0.5). We considered $c$ as a constant in our study, $c = 2.3$. Equation 5 is valid only for non grazing incidences of the magnetic field lines on the collectors. As illustrated in Fig. 1, the angular position of the Gundestrup probe head in the shots studied is such that the pair of pins 4-8 is tangential to the magnetic field within $\pm 2°$. Hence, only the ratios of $I_{sat}$ on pairs 1-5, 2-6 and 3-7 were used for the Van Goubergen fit.

Fig. 8 shows the flow velocity profiles obtained on the way back of the probe's reciprocation. As for the $I_{sat}$ fluctuations and the radial electric field, a clear distinction can be made between the closed field lines region and the SOL. Inside the separatrix, the ECCs at full current are responsible for an increase of the parallel flow velocity away

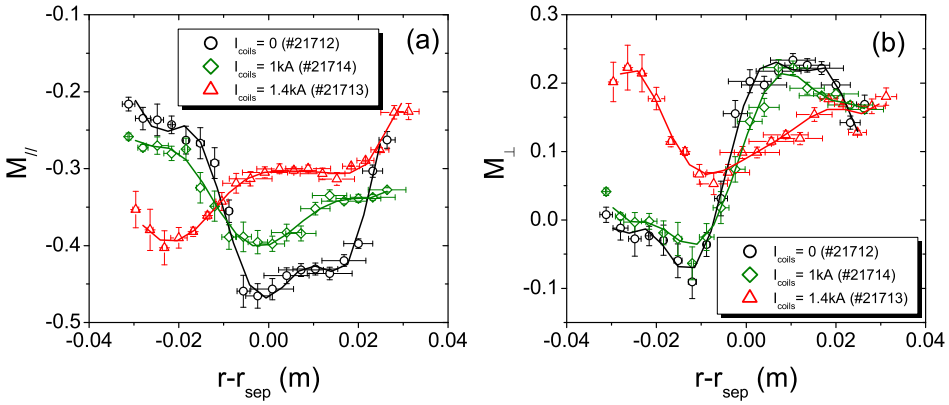


**Figure 8.** (a) Radial profiles of the parallel Mach number $M_{\|}$ as obtained from a Van Goubergen fit of the Gundestrup probe's data during the way back of its reciprocation. $M_{\|} < 0$ corresponds to a parallel flow towards the upper divertor (electron diamagnetic direction). (b) Radial profiles of the perpendicular Mach number $M_{\perp}$. $M_{\perp} > 0$ corresponds to a perpendicular flow towards the lower divertor (ion diamagnetic direction). Polynomial fits are superimposed to guide the eye.

from the lower divertor (electron diamagnetic direction) by $\left|\Delta M_{\|}\right| = 0.15$. The reverse trend is observed in the open field lines region where the parallel flow, although still oriented towards the upper divertor, tends to decrease by $\left|\Delta M_{\|}\right| \sim 0.1$. The same type of behaviour is found for the perpendicular velocity with two opposite trends according to which side of the separatrix is considered. For $r - r_{sep} < 0$, the profiles show a shift of the perpendicular velocity by $\Delta M_{\perp} \sim 0.1 - 0.2$ in the ion diamagnetic direction, while for $r - r_{sep} > 0$ a braking of the rotation by the same amplitude is measured. At $I_{coils} = 1kA$, as one might expect from the previous results, the impact of the RMPs is much less visible although the same trends can be noticed, in particular on the parallel velocity in the SOL. Considering an electron temperature of $T_e = 20eV$ (given by Thomson Scattering) and an ion temperature of $T_i = 60eV$ (order of magnitude found by Retarding Field Analyser measurements in similar discharges), one gets the following order of magnitude for the change in the perpendicular velocity obtained with the Gundestrup data inside the separatrix:

$$\Delta v_{\perp}^{Gundestrup} = \Delta M_{\perp} \sqrt{\frac{T_e + T_i}{m_i}} \sim 5km.s^{-1} \tag{6}$$

With a magnetic field amplitude of $B = 0.35T$ at the location of the probe, it can then be compared to the variation of the ExB velocity that can be inferred from the radial electric field measurement

$$\Delta v_{\perp}^{E_r} = \frac{\Delta E_r}{B} \sim 6km.s^{-1} \tag{7}$$

This way the evolution found of the perpendicular velocity is consistent in direction and amplitude with the variations observed in the radial electric field.

Two other methods demonstrate changes in the perpendicular velocity of the plasma. MAST is indeed equipped with fast visible cameras that make it possible to get an estimate of the perpendicular velocity of filaments by frame to frame correlation [42, 43]. Because of the radial localization of the $D_\alpha$ radiation of the filaments, the velocity calculated using this method correponds to a radial location just outside the separatrix ($r - r_{sep} \sim 0$ to $2cm$). Fig. 9 (a) shows a comparison of the toroidal velocities infered by filament tracking in shots #21287 and #21288 which were based on the same $I_p = 400kA$ scenario as the triplet of shots studied above (the settings used for the cameras in #21712-#21714 were not suitable for the filament tracking techniques). In #21287, the ECCs were energized at full current with the same timing as in #21713, while no perturbation field was applied in #21288. The onset of the RMPs at $t = 0.3s$ leads to a clear braking of the plasma toroidal rotation by $\Delta v_{tor} \sim 2km.s^{-1}$. Projecting on the perpendicular direction (we recall that the pitch angle of the magnetic field lines at the location of the probe is about 21° in those discharges), we get $\Delta v_\perp^{camera} \sim 5km.s^{-1}$, in excellent agreement with the direction and amplitude found with the Gundestrup probe's fit at the same radial location.

The second method used is the cross-correlation between the different $I_{sat}$ signals, which gives some information on the perpendicular velocity of plasma fluctuations. Let us define $\delta t_{i,j}$ $(i, j = 1..8)$ as the position of the peak of the cross-correlation function between pin $i$ and pin $j$. Assuming that $k_\parallel \ll k_\perp$ (ie the fluctuations can be considered as field-aligned filaments) and that the structures do only have a toroidal (or poloidal) velocity (not radial), a simple geometrical calculation yields:

$$\delta t_{i,i+\Delta i} = \tau_{correl}\left(\Delta i\right) . \sin\left(\alpha_i + \frac{\pi}{8}\Delta i\right) \qquad \forall i = 1..8 \quad \forall \Delta i = 0..3 \tag{8}$$

where $\alpha_i$ is the incidence angle of the magnetic field line on pin $i$. $\tau_{correl}\left(\Delta i\right)$ depends on the perpendicular velocity $v_\perp$ via:

$$\tau_{correl}\left(\Delta i\right) = -\frac{2r_p}{v_\perp}\sin\left(\frac{\pi}{8}\Delta i\right) \tag{9}$$

with $r_p = 2.5cm$ the radius of the probe head. The radial profile of $\tau_{correl}\left(1\right)$ is given in Fig. 9 (b) for shots #21712 to #21714. The amplitude of the peak of the correlation functions is also plotted (averaged over the 8 pairs of pins $(i, i+1)$), giving some insight into the goodness of the correlation between the signals. Let us first consider the SOL ($r - r_{sep} > 0$). The amplitude of the correlation functions maxima was found to be ranging from 0.7 to 0.9 demonstrating a good correlation between the pins. This is due to the fact that the assumption of field-aligned filamentary structures is well verified in that region of the plasma as the fast camera images show [42, 43]. Between the $I_{coils} = 0$ and the $I_{coils} = 1.4kA$ cases $\tau_{correl}\left(1\right)$ changes from about $-4\mu s$ to $-7\mu s$. Such an evolution is consistent with the braking found with the Gundestrup probe and the fast camera imaging. It is interesting to note that the RMPs at full amplitude tend to decrease the degree of correlation between the different pins. One could be tempted to associate this effect with a break-down of the largest coherent structures but the absence of any major impact on the PDFs or the spectra (see section 3.1) is hardly

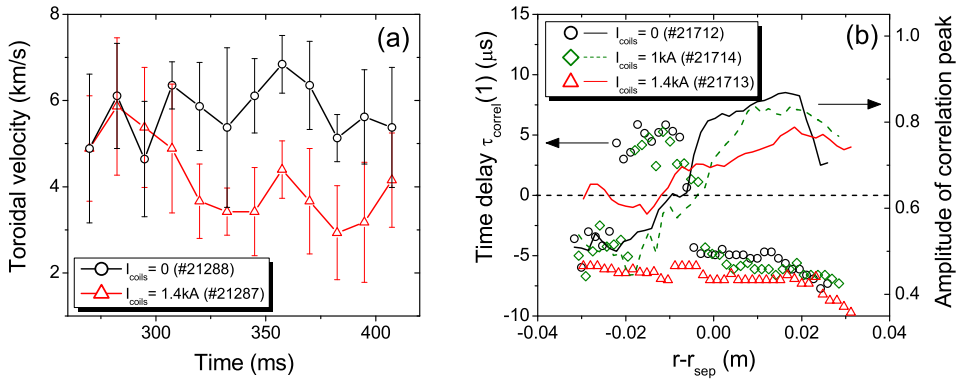


**Figure 9.** (a) Time evolution of the filaments toroidal velocity inferred from filament tracking on fast camera images in shots #21287 ($I_{coils} = 1.4kA$ turned on at $t = 300ms$) and #21288 ($I_{coils} = 0$). (b) Time delay $\tau_{correl}\,(1)$ between the $I_{sat}$ signals measured by two consecutive pins (as defined by Eq. 8) and the amplitude of the correlation peak as a function of the radial position.

compatible with such an explanation. Inside the separatrix, the correlation between the various signals tends to drop as the probe moves deeper into the closed field lines region. This casts some doubt on the filamentary structure assumption. Moreover, one can notice that in the $I_{coils} = 0$ and $I_{coils} = 1kA$ cases, $\tau_{correl}\,(1)$ does not keep a constant sign throughout the profile whereas it does in the $I_{coils} = 1.4kA$ one. The fact that $\tau_{correl}\,(1)$ can go through 0 demonstrates the limit of Eq. 8 and 9 (which would yield an infinite perpendicular velocity) and suggests that a radial velocity should be taken into account for a proper interpretation of the cross-correlation functions in terms of $v_\perp$. This is beyond the scope of this paper. Thus, it is difficult to interpret the correlation data inside the separatrix in terms of plasma fluctuations velocity. However, we can still conclude that the direction of propagation of the structures does not reverse accross a radial profile when the ECCs are energized but does when no current is applied or when $I_{coils}$ is below the threshold to see an effect on the edge plasma. This can be related to the flattening of the perpendicular velocity profiles plotted on Fig.8.

## 4. Discussion

### *4.1. The pump-out, cause or consequence?*

Due to the density pump-out occurring when the ELM coils are powered at full current, the line-averaged density of the plasma during measurements at $I_{coils} = 1.4kA$ (shot #21713) is about 15% lower than in the reference discharge (#21712). This is confirmed by Thomson Scattering data that show a downshift of the whole density profile during the pump-out. Given the observed impact of the RMPs on the edge turbulence characteristics, a possible explanation of the phenomenon would be an enhancement of

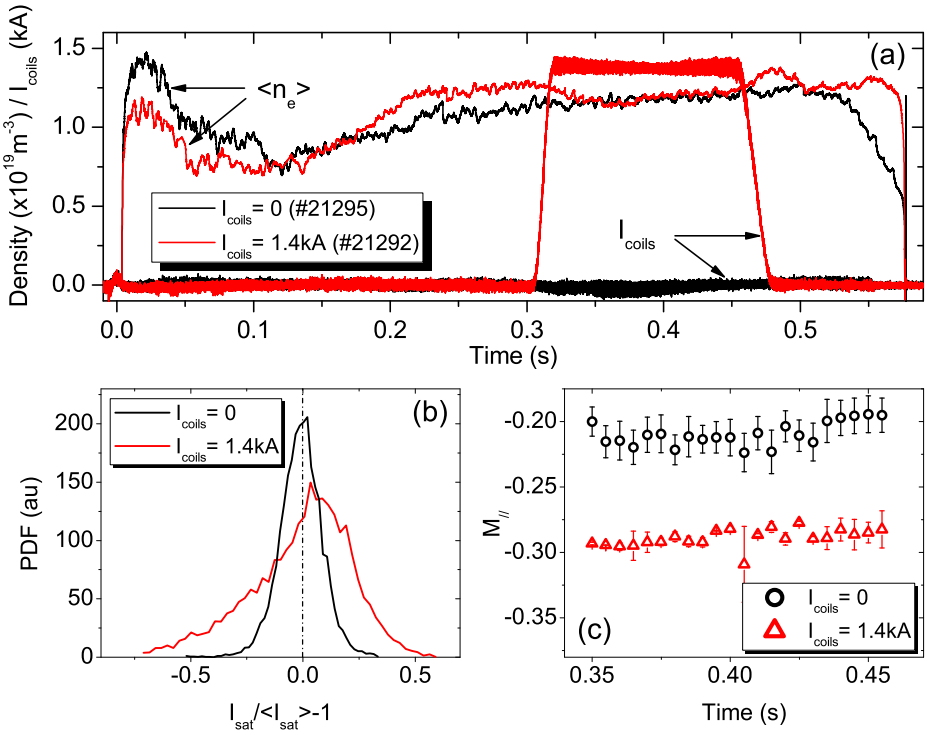


**Figure 10.** Comparison of the data measured at $r - r_{sep} = -2cm$ by the Gundestrup probe in shots #21292 ($I_{coils} = 1.4kA$) and #21295 ($I_{coils} = 0$) with matched line-averaged density during the RMPs phase (a). (b) Probability Distribution Function of the ion saturation current fluctuations measured by pin 2. (c) Parallel Mach number inferred from a Van Goubergen fit.

the particle turbulent transport in the outer plasma due to the magnetic perturbation. However, one might argue that the effects described in the previous section are not directly due to the RMPs, but are just consequences of the lower density.

A pair of shots run with (#21292, $I_{coils} = 1.4kA$) and without (#21295) power in the ECCs gives us an answer to that question. Those two shots are based on the same $I_p = 400kA$ ohmic L-mode scenario as the triplet studied in the previous section. However, the gas injection was set at a lower value in #21295 so that the line-averaged density matched that of #21292 during the ECCs flat-top (Fig. 10 (a)). The reciprocation's settings of the Gundestrup probe were different from those in #21712-#21713 so that the probe remained static at its deepest position in the plasma during the application of the RMPs. Hence we cannot compare profiles but only the impact of the ECCs at a single location in the closed field lines region, which is the radius where their effect is the most noticeable.

Fig. 10 (b) and (c) respectively show the comparison of the PDF of the ion saturation current measured by pin 2 and of the parallel Mach number inferred from

a Van Goubergen fit at $r - r_{sep} = -2cm$ in shots #21292 and #21295 at the time when the ECCs are energized in the former. These 2 plots show that the effect of the RMPs is very similar to those described in the previous section (see Fig. 6 and Fig. 8) with an asymmetrisation of the PDF (development of a negative tail in the case of pin 2) and an increase of the parallel flow velocity in the closed field lines region from $M_{//} = 0.2$ to $M_{//} = 0.3$. The impact of the ECCs on the other analyzed parameters is also quantitatively similar to that observed in #21712-#21713 in the closed field lines region:

- Broadening of the power spectrum of the $I_{sat}$ fluctuations with an increase of the fluctuation level from 10-15% to 18-30% according to the considered pin. Note that the absolute levels are slightly lower than in shots #21712-#21713 due to the lower density in #21292-#21295.
- Asymmetrisation of the PDFs of the $I_{sat}$ fluctuations, the direction of the tail depending on the considered pin.
- Drop of the floating potential by 30V. The probe having been held static in those discharges, we cannot draw any conclusion concerning the radial electric field.
- Increase of the perpendicular Mach number by 0.15.

Hence we can conclude that the observations reported in the previous section are direct consequences of the RMPs and not a side-effect due to the density pump-out.

### *4.2. Effect of the phase of the perturbation relative to the probe's location*

Another natural question that arises when analysing the results of these experiments is that of the toroidal symmetry of the observed effects. Indeed, the magnetic perturbation induced by the MAST ECCs has a dominant $n = 3$ toroidal component and is therefore not toroidally symmetric. In even configuration, the perturbative field in the mid-plane is purely radial, but its sign depends on the toroidal position. The additional radial field might lead to a deformation of the flux surfaces as was already reported on MAST and JET using error field correction coils [44]. One may also expect this radial component of the field to interact with the plasma current to generate a vertical $\mathbf{j} \times \mathbf{B}$ force leading to a vertical shift of the plasma with an $n = 3$ symmetry. From that point of view, some of the effects of the RMPs described above could be interpreted as consequences of a local radial or vertical shift of the plasma. Even though previous studies on MAST did conclude that the properties of the edge turbulence are independent of the edge magnetic field configuration [45], the discharges studied in this paper are based on a different scenario and so this ansatz is worth investigating. This can be done by looking at the toroidal symmetry of the effects of the RMPs.

Rather than changing the toroidal location of the reciprocating probe (which is actually not possible), we took advantage of the flexibility of the ECCs configuration to carry out such a toroidal symmetry analysis. Under the assumption that the only toroidally asymmetric actuator influencing the plasma are the RMPs, changing the

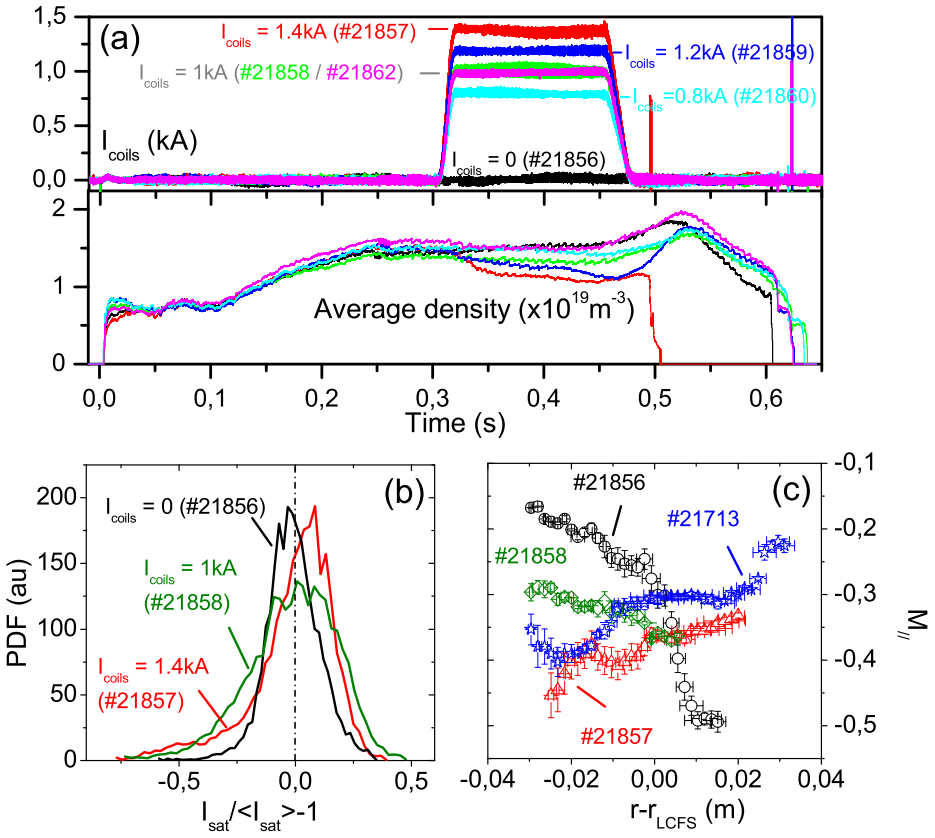


**Figure 11.** (a) Time traces of the current applied in the ELM Control Coils and of the plasma average density for the set of shots run in 0° phase. (b) PDF of the ion saturation signal measured by pin 2 at $r - r_{sep} = -2cm$ for $I_{coils} = 0$ (#21856), $1kA$ (#21858) and $1.4kA$ (#21857). (c) Parallel Mach number profiles inferred from a Van Goubergen fit on the way back of the Gundestrup probe's reciprocation. Profiles for shots #21856 ($I_{coils} = 0$ - black circles), #21858 ($I_{coils} = 1kA$ - green diamonds) and #21857 ($I_{coils} = 1.4kA$ - red triangles) are shown and compared with the profile measured in #21713 ($I_{coils} = 1.4kA$, 60° phase - blue stars).

phase of current in the ECCs from 60° to 0° phase is equivalent to changing the toroidal location of the reciprocating probe by 60°. In 60° phase, the radial component of the perturbation at the toroidal location of the reciprocating probe is negative; in 0° phase, it is positive.

A series of $I_p = 400kA$ ohmic L-mode CDN discharges were run with the ECCs in even parity 0° phase configuration with the following values for the drive current: $I_{coils} = 0$ (#21856), $I_{coils} = 0.8kA$ (#21860), $I_{coils} = 1kA$ (#21858 and #21862) and $I_{coils} = 1.4kA$ (#21857) (Fig. 11 (a)). The density pump-out is clearly visible on the density traces, which was expected since a change in the phase should not change anything on the global response of the plasma. However, one noticeable difference compared with the triplet #21712 to #21714 is the existence of a pump-out even at

$I_{coils} = 1kA$. Indeed, in the set of discharges #21856 to #21862, the threshold on the ECCs current necessary to see any effect seems to be lower, probably around 0.8kA. Such a difference may in fact be related to a slight density difference: the set of discharges run with the coils in 0° phase has an average density 10% lower than those run in 60° phase. An effect of the density on the amplitude of the pump-out has already been reported in ref. [11].

The PDFs of the $I_{sat}$ fluctuations measured by pin 2 are shown in Fig. 11 (b) for the $I_{coils} = 0$, $1kA$ and $1.4kA$ cases. The same evolution as in 60° phase can be observed, with the PDF developing a negative tail when applying the RMPs. This time (contrary to shot #21714), the $I_{coils} = 1kA$ case already shows an effect, demonstrating that the pump-out and the modification of the fluctuation characteristics probably have the same threshold. Fig. 11 (c) gives the parallel Mach number profiles measured in the same three discharges. The profile measured in #21713 ($I_{coils} = 1.4kA$, 60° phase) is also plotted for comparison. The impact of the RMPs on the parallel flow velocity is quantitatively similar to that found in 60° phase with a flattening of the profile leading to an acceleration in the closed field lines region and a braking in the SOL. Once again, the only noticeable difference with the case plotted in Fig. 8 is the existence of an intermediate effect at $I_{coils} = 1kA$ linked to the lower density and the associated lower threshold on the coils current. As in section 4.1, the impact of the RMPs on the other observed quantities (power spectra of $I_{sat}$ fluctuations, $E_r$, $M_\perp$) was found quantitatively comparable to that measured in #21712-#21714. We hence conclude that the phase of the coils has no effect on the impact of the RMPs measured by the reciprocating probe, thus demonstrating that the phenomena reported in section 3 are not localized in the toroidal direction.

### *4.3. Comparison with results on other machines*

Let us now compare our results with those found during ergodic divertor experiments on other machines. A strong common feature of all these experiments is the increase of the floating potential measured by Langmuir Probes in the ergodic layer inside the separatrix when the RMPs are applied [15, 19, 21, 22]. This change leads to an increase of the radial electric field which, in turn, drives a modification of the poloidal rotation [20, 24, 21, 22]. These results are qualitatively similar to what we measured in MAST.

Concerning the impact of the RMPs on the edge transport during ergodic divertor experiments, the comparison is not so straightforward. Experiments in Tore Supra [19] showed an important drop of the electron temperature at the very edge of the closed field lines region and in the SOL, while the density profile as well as both fields' profiles in the core were not modified. A similar drop of $T_e$ was observed in TEXTOR [21]. On the contrary, in MAST, the ECCs impact mainly the density while no noticeable modification was observed on the temperature profiles. Looking at fluctuations, a reduction of the fluctuations level was observed in the SOL of both Tore Supra [20] and TEXTOR [23] with little change of the PDF. Such a result is similar to what we

report here. In the closed field lines region however, our measurements show an increase of the fluctuations level and a broadening of the power spectra in contradiction with what was observed in Tore Supra [19] and TEXTOR [22]. Hence, the mechanisms at play in MAST are probably different. Explaining these differences is out of the scope of this paper. Nevertheless, the reason for such discrepancies could be found in the difference in the edge configurations of the 3 machines, MAST being the only one having an X-point (in fact two in double-null configuration).

## 5. Summary

The impact of the ELM Control Coils (ECCs) on the edge plasma of the MAST spherical tokamak has been studied using a Gundestrup reciprocating probe in 400kA ohmic L-mode plasmas. These discharges exhibit a density pump-out when the ECCs are energized above a given current threshold. Under that threshold, no major impact of the ECCs was observed on any of the measured quantities. Above the threshold, however, the edge plasma is strongly perturbed by the RMPs with a different impact whether closed flux surfaces or open flux surfaces (within a $5cm$ range across the separatrix) are considered. Table 1 gives a summary of the observations made. Two natural questions arise from those results. The first one deals with the toroidal localization of the observed effects. Experiments run with a different phasing of the coils with respect to their position in the vessel demonstrated that the impact of the ECCs is not toroidally localized and in particular not due to a local vertical or radial shift of the plasma. The second question is that of the cause to effect link between the pump-out and the other phenomena. A set of discharges run with matching densities during the RMPs phase ruled out the assumption that the density drop could be the main cause of the changes measured in the fluctuations, radial electric field or velocity profiles. Given that the pump-out and these phenomena appear to have the same existence threshold in terms of current in the ECCs, it is however legitimate to assert that they are related. In particular, the alteration of the fluctuation characteristics is the sign of a modification of the turbulent transport level that could explain the pump-out as well as the modification of the flows [46]. Although our results show some important similarities with those obtained during ergodic divertor operation in other machines, in particular the increase of the radial electric field when the RMPs are applied, the impact of the ECCs on the edge fluctuations is very different from what was observed in these experiments. This suggests that the physics at play in the interaction between the RMPs and the turbulent transport are probably not the same. Further studies investigating the nature of the turbulence as well as the radial turbulent flux would be necessary to complete the present dataset and give a coherent physical picture of the impact of the ECCs on the plasma.

| | Inside the separatrix | In the SOL |
|---|---|---|
| Ion saturation current fluctuations | • Broadening of the power spectra<br>• Increase of the fluctuation level of the order of 50%<br>• Asymmetrisation of the probability distribution functions similar to what is observed in the SOL without RMPs | • Decrease of the fluctuation level of the order of 10%<br>• No major impact on the PDF or the spectra |
| Radial electric field | Increase by $\sim 2kV/m$ | Decrease by $\lesssim 1kV/m$ |
| Flow velocities ($M_\parallel > 0$ = towards lower divertor) ($M_\perp > 0$ = towards upper divertor) | • Decrease of $M_\parallel$ by $\sim$ 0.15<br>• Increase of $M_\perp$ by $\sim$ 0.15 leading to the disappearance of the flow reversal observed without the ECCs<br>• The disappearance of the flow reversal is confirmed by cross-correlation analysis | • Increase of $M_\parallel$ by $\sim$ 0.15<br>• Decrease of $M_\perp$ by $\sim$ 0.1<br>• Braking of the perpendicular rotation confirmed by filament tracking with fast cameras |

**Table 1.** Summary of the impact of the Resonant Magnetic Perturbations imposed by the ELM Control Coils in the studied $I_p = 400kA$ ohmic L-mode scenarios.

## Acknowledgments

This work was funded by the United Kingdom Engineering and Physical Sciences Research Council under grant EP/G003955 and the European Communities under the contract of Association between EURATOM and CCFE. The views and opinions expressed herein do not necessarily reflect those of the European Commission.

## References

[1] R. Hawryluk et al., Nucl. Fusion **49**, 065012 (2009).

[2] K.H. Burrell et al., Plasma Phys. Control. Fusion **47**, B37-B52 (2005).
[3] T.E. Evans et al., Nucl. Fusion **48**, 024002 (2008).
[4] M.E. Fenstermacher et al., Phys. Plasmas **15**, 056122 (2008).
[5] O. Schmitz et al., Plasma Phys. Control. Fusion **50**, 124029 (2008).
[6] Y. Liang et al., Phys. Rev. Lett. **98**, 265004 (2007).
[7] Y. Liang et al., Plasma Phys. Control. Fusion **49**, B581 (2007).
[8] J.W. Connor, Plasma Phys. Control. Fus. **40**, 531-542 (1998).
[9] G.T.A. Huysmans, Plasma Phys. Control. Fus. **47**, B165-B178 (2005).
[10] E. Nardon et al., J. Nucl. Mater. **390-391**, 773 (2009).
[11] E. Nardon, 36th EPS Conference on Plasma Physics, accepted Plasma Phys. Control. Fus. (2009).
[12] H.R. Strauss et al., Nucl. Fusion **49**, 055025 (2009).
[13] M.F. Heyn et al., Nucl. Fusion **48**, 024005 (2008).
[14] E. Nardon et al., accepted Nucl. Fusion (2010).
[15] S.C. McCool et al., Nucl. Fusion **29**, 547 (1989).
[16] Ph. Ghendrih, A. Grosman and H. Capes, Plasma Phys. Control. Fus. **38**, 1653-1724 (1996).
[17] Ph. Ghendrih et al., Nucl. Fusion **42**, 1221 (2002).
[18] K.H. Finken et al., Plasma Phys. Control. Fus. **46**, B143 (2004).
[19] J. Payan et al., Nucl. Fusion **35**, 1357 (1995).
[20] P. Devynck et al., Nucl. Fusion **42**, 697-707 (2002).
[21] Y. Xu et al., Phys. Rev. Lett. **97**, 165003 (2006).
[22] Y. Xu et al., Nucl. Fusion **47**, 1696-1709 (2007).
[23] Y. Xu et al., Nucl. Fusion **49**, 035005 (2009).
[24] B. Unterberg et al., J. Nucl. Mater. **363-365**, 698-702 (2007).
[25] M.F.M. De Bock et al., Nucl. Fusion **48**, 015007 (2008).
[26] P.C. Stangeby, The Plasma Boundary of Magnetic Fusion Devices, IoP, (2000).
[27] Y. Yang, G.F. Counsell and the MAST team, J. Nucl. Mater. **313-316**, 734 (2003).
[28] C.S. MacLatchy et al., Rev. Sci. Instrum. **63**, 3923 (1992).
[29] A. Kirk et al., accepted Nucl. Fusion (2010).
[30] L. Lao et al., Nucl. Fusion **25**, 1611 (1985).
[31] R.A. Moyer et al., 21st IAEA Fusion Energy Conference, Chengdu, http://www-naweb.iaea.org/napc/physics/FEC/FEC2006/html/node415.htm#82745 (2006).
[32] V. Rozhansky et al., accepted Nucl. Fusion (2010).
[33] S.J. Zweben et al., Plasma Phys. Control. Fus. **49**, S1-S23 (2007).
[34] M. Kočan et al., Plasma Phys. Control. Fus. **50**, 125009 (2008).
[35] H. Meyer et al., Journal of Physics: Conference Series **123**, 012005 (2008).
[36] D. Temple et al., 36th EPS Conference on Plasma Physics P5.191, Sofia (2009).
[37] H. Van Goubergen et al., Plasma Phys. Control. Fus. **41**, L17 (1999).
[38] I.H. Hutchinson, Phys. Fluids **30**, 3777 (1987).
[39] K.-S. Chung and I.H. Hutchinson, Phys. Rev. A **38**, 4721 (1988).
[40] J.P. Gunn et al., Phys. Plasmas **8**, 1995 (2001).
[41] I.H. Hutchinson, Principles of Plasma Diagnostics, Cambridge University Press (2002).
[42] B.D. Dudson et al., Plasma Phys. Control. Fus. **50**, 124012 (2008).
[43] N. Ben Ayed et al., Plasma Phys. Control. Fus. **51**, 035016 (2009).
[44] I.T. Chapman et al., Nucl. Fusion **47**, L36-L40 (2007).
[45] B. Hnat et al., Nucl. Fusion **48**, 085009 (2009).
[46] P. Tamain et al., J. Nucl. Mater. **390-391**, 347-350 (2009).